Elongated soy protein isolate-poly(D, L-lactide-co-glycolic acid) microcapsules prepared using syringe filters and their effect on self-healing efficiency of soy protein-based green resin

Shanshan Shi
Cornell University
Anil Netravali (ann2@cornell.edu)
Cornell University

Research Article

Keywords: Self-healing, membrane-emulsification, elongated microcapsules, green resin, soy protein

Posted Date: March 8th, 2022

DOI: https://doi.org/10.21203/rs.3.rs-1354092/v1

Abstract

A self-healing soy-based resin filled with soy protein isolate (SPI) containing poly(D, L-lactide-co-glycolic acid) (PLGA) microcapsules (MCs) was prepared. MCs were prepared using a syringe filter via a membrane emulsification technique. Using this method, spherical (diameter of about 1.30 μm) and elongated MCs (aspect ratios up to 20) could be produced. Tensile properties and self-healing efficiencies of resins were characterized for both MC morphologies in terms of strength recovery and toughness recovery. While both MCs could successfully heal cracks, spherical MCs were seen to compromise the tensile properties of the resin, whereas elongated MCs demonstrated some mechanical enhancement. Overall results showed that elongated MCs having a higher aspect ratio resulted in slightly better self-healing performance as well as a mechanical improvement. The results also show that higher MC loading results in higher self-healing efficiency.

1 Introduction

In the last half-century, the world witnessed a 200-fold growth in the production and utilization of plastics [1]. Most plastics at present are synthesized using petroleum as the raw material. It has been estimated that the earth will run out of petroleum within the next 5–6 decades if the current consumption rate continues [2]. Additionally, the ultimate fate of these plastics has become one of the most critical concerns human civilizations are facing. Most petroleum derived synthetic plastics do not degrade in nature for several centuries. Even though there are considerable efforts to recycle plastics or incinerate them to get the energy value, the majority of them get dumped in landfills or oceans, severely disrupting the entire ecosystem [1].

Efforts to explore renewable substitutes, primarily derived from sustainable and yearly renewable biomass, have grown in the past decade at a rapid pace worldwide. Plant-based soy protein has been considered as one of the top green raw material sources because of its worldwide availability at an economical price. One such raw material, soy protein isolate (SPI) containing about 92% protein, is commercially available [3]. It also exhibits high solubility in water facilitating green processing. SPI has also been shown to quickly degrade when exposed to compost medium, fully eliminating the need for landfills. These characteristics make SPI an excellent feed source for plastics [3].

Apart from developing inexhaustible or fully renewable materials, prolonging the service life of current polymers and their products, including the bio-based ones, could also alleviate the serious plastic disposal problem we currently face. Incorporating self-healing characteristics in green resins and composites would be one way that would not only maximize the longevity of these materials and lower maintenance costs but also improve their safety and promote further sustainability. However, green materials with self-healing properties have not been well studied [4]. Kim and Netravali successfully prepared SPI resins [5] and starch resins [6] with (SPI)-poly(D, L-lactide-co-glycolic acid) (PLGA) microcapsules (MCs) that demonstrated good self-healing properties.

The spherical MC-based self-healing system was the first self-healing system developed. It is also one of the most successful self-healing systems that can autonomously restore the mechanical properties of polymer resins [7]. Microencapsulation has been the most widely used method to prepare MCs that contain healant, where emulsification is a critical procedure in MC preparation. Many emulsification methods, including membrane emulsification [8, 9], high-pressure homogenization [10], ultrasound emulsification [11], and application of copolymer, have been developed [12]. Kim and Netravali prepared SPI-PLGA MCs using high-pressure homogenization to build a W/O/W emulsion system and embedded them into the SPI composites [5]. Their results showed composites with about 30% self-healing efficiency. Membrane emulsification, particularly with Shirasu porous glass (SPG) membrane, has been widely used to prepare emulsions due to its ability to produce MCs of uniform sizes [8,9,13]. SPG membranes, however, are expensive. Instead of using such expensive membranes, the present research used a commercially available syringe-filter as the membrane template, as a substitute for SPG membrane, to set up a waster in oil in water (W/O/W) double emulsion system. This modification can not only reduce production cost and time but also can produce MCs within a narrow size range, which is very desirable for uniformly dispersing them in the resin. More importantly, different morphologies of MCs can be produced by manipulating parameters such as pump rate and pore sizes of the syringe filters. Elongated MCs can increase the probability of the MCs being in the path of the microcracks as well as enhance MC/resin adhesion [14, 15]. Both these factors could potentially boost the self-healing efficiency.

Polyvinyl alcohol (PVA) has been widely used as a stabilizer in emulsion systems. However, it has also been studied as a ‘link’ connecting MCs with resins and increasing MC/resin interaction [16]. The hydrocarbon part (CH_2CH) of the PVA can get attached to the PLGA shell via hydrophobic interactions while the hydrophilic region extends into the SPI resins, boosting the MC/resin interaction [16]. It was shown that the combination of the PVA-aided hydrogen bonding on the surface of the SPI-PLGA MCs and the elongated MCs creates a positive impact on both the self-healing performance and the mechanical performance [5].

2 Materials And Methods

2.1 Materials

Soy protein isolate (SPI), ProFam 974, was provided by Archer Daniels Midland Company, Decatur, IL. Poly (DL-lactide-co-glycolide) (50:50, ester-terminated PLGA) was purchased from the Division of DURECT Corporation, Birmingham, AL. Two inherent viscosities of 1.15 dL/g and 1.20 dL/g of PLGA in hexafluoroisopropanol were obtained depending on the goods in stock. Both worked equally well and were used interchangeably. Poly (vinyl alcohol) (PVA, average Mw 31,000–50,000, 98–99% hydrolyzed), sodium hydroxide pellets (NaOH, 97.0%), glutaraldehyde (GA, 25 wt% solutions in water), ethyl acetate (EA, ≥ 99.8%), and polyvinylpyrrolidone (PVP), Rhodamine B (powder) and Bradford reagent (0.1%), Coomassie blue R-250 solution (composed of 45% methanol, 10% acetic acid and deionized (DI) water in the ratio 5:4:1) and sodium dodecyl sulfate (SDS) were purchased from Sigma-Aldrich (St. Louis, MO).

2.2 Preparation of MCs

The present research used a W/O/W double emulsion method to prepare microcapsules [5]. SPI/water solution, the healant, was encapsulated in PLGA shells. To prepare the healant, 100 mL of SPI/water solution (0.15 g/mL) was denatured using 10 mL of a 4 M NaOH solution at 80 ℃ and 300 rpm for 15 min. Prepared SPI solution (10 mL), healant, and separately prepared PLGA/EA solution (30 mL, 0.01 g/mL) were stirred at the highest power of the vortex mixer (BenchMixer) for 10 min to form a W/O inverted emulsion. As explained below, MCs with two morphologies, spherical and elongated, were produced.

2.2.1 Producing spherical MCs using the syringe-filter method (abbreviation: SF-I)

The prepared W/O emulsion was then extruded through a 0.45 μm-syringe filter and a 25-gauge 50-mm needle (the device set-up is shown in TOC figure) using a dual-syringe pump (PHD ULTRA, Harvard Apparatus, MA, USA) at the rate of 3 mL/min into 80 mL of 5 wt% PVA/water solution while being stirred. The entire mixture was stirred at 300 rpm at room temperature (RT) during the extrusion. The mixture was kept stirring overnight to allow complete evaporation of EA, and the MCs that formed were collected by centrifuging the mixture at 5000 rpm (Thermo Scientific Super-Nuova) for 10 min. The MCs were washed with deionized (DI) water twice before freeze-drying at -82℃ for 24 h.

2.2.2 Producing elongated MCs using the syringe-filter method (abbreviation: SF-II)

Elongated MCs were produced in a slightly different way from spherical MCs. As is shown in the TOC, a 25 gauge, blunt-end, 80 mm long needle was used to generate the elongated MC shapes. The W/O emulsion was pumped (extruded) at the rate of 1 mL/min into a 200 mL glass beaker containing 80 mL of 5 wt% PVA water solution. The entire mixture was stirred at 300 rpm at RT during the extrusion. The mixture was kept stirring overnight to evaporate EA fully, and the elongated MCs were collected by centrifuging the mixture at 5000 rpm for 10 min. The MCs were washed with DI water twice before freeze-drying at -82℃ for 24 h. Elongated MCs were assumed to be formed while traveling along the long path of the 25-gauge needle.

2.3 Preparation of SPI based self-healing green resins

Self-healing green resins were prepared simply by mixing denatured SPI/water solution and different amounts of MCs and then crosslinking SPI with GA as reported. Briefly, 10 g SPI was dissolved and denatured in 8% NaOH solution for 15 minutes. Then a series of loadings of MCs (0, 5, 10, 15, 20, 30 wt% of SPI powder) was suspended, separately, in the denatured SPI solution 10 min before crosslinking with 20 wt% of GA. Twenty minutes later, the solution was poured into Teflon® coated molds and cured overnight in the oven at 75℃ in the form of sheets. To obtain uniform thickness, SPI resin sheets were processed using the hot-press machine with a set pressure at 0.09 MPa at 80℃ for 10 min using 1 mm

spacers. As per ASTM E647-08 [17], resin specimens for self-efficiency tests were cut into desired shape as shown in Fig. 1(a) [14]. Specimens were kept in a desiccator to remove excess moisture and prevent further moisture absorption for three days before performing self-healing efficiency tests.

2.4 Characterization of the MCs

2.4.1 Scanning electron microscope (SEM) analysis

SEM (Leo 1550 SEM, and Zeiss Gemini 500 FESEM) was used to characterize the shapes, sizes, morphologies, and surface topographies of MCs. MCs were resuspended in water and a drop of the suspension was deposited on a conductive carbon tape that was glued to the SEM stub and dried before being coated with gold.

2.4.2 Evaluation of protein loading in MCs

The protein loading in the MCs was determined using the protocol reported by Hora et al. [18]. Briefly, MCs (100 mg) were milled into powder to release SPI slurry, and the powder was added to 10 mL of 10 mM NaOH, which contained 5% (w/v) SDS. The suspension was centrifuged at 5000 rpm for 10 min to discard the insoluble residue. A standard calibration curve was set up using a series of standard SPI solutions. SPI solutions were prepared with concentrations ranging from 10 mg/mL to 0.1 mg/mL using a ten mM NaOH solution. Then a desired amount of the Bradford agent was added to all standard SPI solutions and samples (pH = 2, 0.5 mM HCl adjusted), respectively, until a blue color was observed. The protein loading was calculated at the maximum absorption at 595 nm using a UV/Vis spectrophotometer (Perkin-Elmer Lambda 35) [18].

2.4.3 Confocal laser scanning microscope (CLSM) analysis

CLSM (Zeiss LSM 710) was employed to analyze the core-shell structure. The SPI slurry was dyed using Rhodamine B water solution (1 wt%) before emulsification. MCs were prepared using the same process described above in section 2.2. A 63X oil-immersion lens and the associated filter (514 nm wavelength excitation) were used to characterize MCs.

2.4.4 Attenuated total reflection–Fourier transform infrared (ATR-FTIR) analysis

ATR-FTIR (Magna 560, Nicolet Instrument Technologies, Fitchburg, WI, USA) with split pea accessory was used to analyze SPI-PLGA MC chemical content. Each sample batch was scanned from 4000 cm^{-1} to 500 cm^{-1} with three repeats to assure data integrity.

2.5 Characterization of self-healing SPI resins

2.5.1 SEM characterization

Fracture surfaces of all resin specimens were characterized using SEM after mounting them vertically on double-sided conductive carbon tapes glued to the metal stub as shown in Fig. 1(c) [14].

2.5.2 Tensile characterization

The stress vs strain plots from which fracture stress, fracture strain, and Young's modulus values were obtained using an Instron universal tester (Instron, Model 5566). Resin specimens were cut into strips with dimensions of 50 mm × 10 mm × 1 mm using a shear cutter for tensile tests. The gauge length and crosshead speed were set to 30 mm and 3 mm/min (0.1 min^{-1} strain rate), respectively. All specimens were kept at ASTM conditions of 21°C and 65% relative humidity (RH) for three days prior to conducting the tests.

2.5.3 Self-healing efficiency tests

As shown in Figs. 1(b) and (c), the self-healing efficiency tests were conducted in five steps: I) mounting specimens on Instron; II) pulling the specimen to create a 10 mm crack in the specimen (up to the mouth-shaped arc); III) removing specimens from Instron, pressing the edges of the crack back together and allowing specimens to heal for 24 h in a sealed container; IV) remounting the healed specimens in Instron and pulling them to reopen the 10 mm crack; V) continuing to pull until the specimen breaks into two pieces. The crosshead speed for these tests was set at 0.3 mm/min, the same as before, as per ASTM E647-08 [17].

Self-healing efficiency of the resin was defined as the ratio of the fracture toughness of the healed resin and the virgin resin, as shown in Equations 1 and 2 [14, 19]. The *F* and *F'* correspond to the strength (resin failure load) in the first test and the second test, respectively, at the same displacement, and *T* and *T'* correspond to the toughness (yellow areas shown in Figs. (b) and (c) [14]) in the first and the second tests, respectively, at the same displacement [14].

$$\eta_T = \frac{T' - T}{T} \times 100$$

1

$$\eta_F = \frac{F' - F}{F} \times 100$$

2

3 Results And Discussion

3.1 Morphologies and topographies of SPI-PLGA MCs

MC sizes and their shell wall thicknesses were determined by randomly selecting MCs within the SEM images taken, using Image J software.

Figures 2(a), (c), and (d) show SEM images of SF-I MCs obtained via the syringe-filter method. As can be seen, most MCs are spherical and intact, while a few are broken. The average diameter of MCs in this case (N > 150) was 1.30 μm ± 0.71 μm, and the diameters varied from 0.44 μm to 5.71 μm. The thickness of the shell (N > 100) in this sample ranged between 0.1 μm and 0.25 μm. Figure 2(b) presents the histogram of the size distribution of SF-I MCs. It can be seen from Fig. 2 that most MC diameters fall within a narrow range of 0.5 μm to 1.8 μm. A few sub-micrometer capsules (the smaller MCs) and a few broken MCs can also be seen in Fig. 2(b). Typically, sub-micrometer capsules and broken MCs are undesirable in the preparation of MCs as they do not help the self-healing of the resin but can be detrimental to the mechanical properties of the resins if added.

Figures 3(a), (c), and (d) show typical SEM images of SF-II SPI-PLGA MCs prepared by the syringe-filter method. In this case, the MCs possess a wide range of aspect ratios (from 1 to 20) and a mix of distinctive shapes that include spherical, rod-like, dog-bone-like, and spindle-like. The highest aspect ratio observed from the SEM results was around 20. The elongated morphologies were believed to be shaped by the 80 mm long needle during the MC preparation process. MCs with elongated shapes have the potential to store more healing agents and enhance self-healing efficiency [14, 15]. Significantly, their longer lengths increase the probability of them being in the path of the microcracks. This higher probability can be expected to result in higher self-healing efficiency. It is also possible that elongated MCs can act as reinforcement to improve the mechanical properties of a resin, particularly if the shell strength is high and MC/resin bonding is good. However, a higher strength of the MC shell can reduce the self-healing efficiency by preventing shells from fracturing and releasing the healant.

In terms of the shapes of the MCs, spherical MCs dominate the overall mix of the MCs. An average diameter of 11.64 μm ± 5.01 μm (N > 200) was observed in this sample, which was almost nine times as large as those in the SF-I sample, which had an average diameter of 1.30 μm. The reason leading to larger MC is perhaps combining of MCs along the needle pathway, as shown in confocal images in the following discussion. Figure 3(b) shows the size distribution histogram of intact spherical MCs ranging from 5 to 15 μm, in length.

3.2 Protein loading analysis

Protein loading in SF-I was calculated to be 4.07 wt% while SPI loading in SF-II reached 10.02 wt% as MCs in SF-II were much larger (11.64 μm compared to 1.30 μm) than those in SF-I. It is known that the loading ratio of SPI-PLGA MCs can never exceed the feeding ratio (protein concentration of 13.67 wt%) [14].

3.3 Confocal laser scanning microscopy (CLSM)

Figures 4(a) and (b) show CLSM images of SPI-PLGA SF-I MCs in fluorescent and transmission modes, respectively. The yellow color in the MCs seen in Fig. 4(a) indicates the presence of SPI and hence, confirms that the MCs indeed contain SPI slurry. Both Fig. 4(a) and (b) further confirm the core-shell structure of the MCs.

Figure 5 presents CLSM images showing internal structures of SF-II MCs. Figures 5(a) and (c) show fluorescent images of the MCs, while Figs. 5(b) and (d) show transmission images. From all images seen in Fig. 5, it can be confirmed that SF-II elongated MCs are loaded with SPI protein in spite of their different shapes. As seen in both images in the transmission mode (b) and (d), black dots can be seen within some elongated MCs. These could either be smaller sub-MCs that get incorporated in the bigger MCs or they could be air bubbles. Corresponding fluorescent images (a) and (c) show the contours of elongated MCs and confirm the existence of sub-MCs or air bubbles within the larger MCs. These results are similar to those shown earlier by Kim and Netravali [5].

3.4 ATR-FTIR analysis

Figure 6 shows spectra of PLGA, SPI, PVA, and prepared SF-I and SF-II MCs. Signature absorbance peaks of different functional groups are demonstrated by these ATR-FTIR spectra. For example, a distinguishable carbonyl (C = O) peak at 1725 cm^{-1} can be seen in the PLGA spectrum. Both SF-I and SF-II MCs show a strong peak at 1725 $cm^{-1,}$ indicating the presence of PLGA (shell) on the surfaces as can be expected [20]. Similarly, a peak belonging to bending vibration for the amine group (NH_2) from 1550 to 1650 cm^{-1} can be seen in SPI, SF-I, and SF-II spectra [21]. Spectra for PVA, SPI, SF-I, and SF-II MCs demonstrate an absorption peak at around 2900 cm^{-1} for the valence C-H vibration [22]. Furthermore, an aliphatic -CH_2- peak appears in PVA as well as in the spectra of SF-I and SF-II MCs at 750 to 850 cm^{-1} [23]. These spectra confirm the presence of both SPI and PVA on the surfaces of SF-I and SF-II MCs.

3.5 SEM analysis

To demonstrate self-healing behaviors clearly, resins with the highest loading of MCs were tested for self-healing efficiency. Specifically, SPI resins loaded with 15 wt% SF-I MCs and 30 wt% of SF-II MCs were chosen to study their self-healing behavior.

Figure 7 shows typical SEM images of the microcracks, and fracture surfaces of resins loaded with 15 wt% spherical SF-I MCs. The released healant (SPI) is seen flowing out from SF-I SPI-PLGA MCs in both Figs. 7(a) and (b). While self-healing occurs in the microcrack, in this case, the amount of healant, SPI, seems insufficient to fill the microcrack. Filling the microcrack with the healant is critical for healing it. The volume between two fracture surfaces is overwhelmingly larger than the limited amount of healing agent available from the MCs. Since more healant is needed to fill the microcrack, it could be problematic to have a low loading, i.e., a limited number of MCs in the resin. However, increasing the size (diameter) of MCs or having higher MC loading to obtain more healant, can reduce mechanical properties, i.e., this could be at the expense of the mechanical properties of the resin [5, 14]. Figure 7(c) shows the smooth surface of an unbroken SF-I spherical MC on the fracture surface, which suggests that the bonding between MCs and the resin was not strong enough. Spherical MCs may also be prone to easily debond from the resin at the microcracks rather than fracturing. While PLGA is hydrophobic, having low surface energy, SPI resin is hydrophilic, having high surface energy, it is possible that the bonding is not as desired.

Figure 8 displays typical SEM images of microcracks and fracture surfaces in resins loaded with 30 wt% of SF-II MCs. Many bridges between the two fracture surfaces can be identified in Figs. 8(a) to (c) with different crack sizes where the healant has burst out as a result of microcracks fracturing the MCs. The crosslinking of the healant happens quickly once it gets in contact with the excess GA present in the resins. The elongated MCs were designed to store more healing agent and enhance the mechanical performance of resins. However, as stated earlier, with higher aspect ratios, elongated MCs also increase the probability of being in the path of the microcracks, assuring their fracture and, thus, increasing the self-healing efficiency [14, 15].

Figure 8(d) demonstrates a resin failure mode in which a microcrack propagates within the resin along the edge of an elongated MC without fracturing it. This failure mode can occur when the microcracks run along the length, rather than across, the MCs. While the MCs are randomly oriented within the resin, such situations can result in lower self-healing efficiency and compromise the mechanical performance of the structural composites. From Fig. 8(d), one can conclude that the MC/resin interfacial bonding was insufficient to withstand the shearing at the MC/resin interfacial boundaries. Similar situations can be seen in Figs. 8(e) and (f). A small gap between the healant and the MC shell observed in the SEM image shown in Fig. 8(f) confirms weak bonding between MCs and resins.

3.6 Mechanical properties

A two-tailed unequal variance t-test was utilized for statistical analysis and a 95% confidence interval was chosen. Data for failure load are shown as histogram of means ± standard deviation. The effect of SF-I and SF-II MC loading on the resin failure load (an indicator of strength) during the self-healing efficiency tests are depicted in Fig. 9(a). All resins showed that there is an optimum MC loading (wt%) beyond which the strength of the resin drops, which is similar to what was observed by earlier researchers for the soy protein-based resin [5, 6, 14]. They suggested that at higher loadings, MCs start to aggregate, forming significant defects which affect their tensile properties. From Fig. 9, it can be concluded that resins loaded with SF-I MCs showed minor enhancement in the failure load of the resins at a low loading of 5% in the case of SF-I MCs. Additional MC loading, however, reduced the failure load (strength), i.e., the overall mechanical performance of the resin. Resins with SF-I MCs showed comparable displacement while reduced load at the break with increased MC loading. The load at break of resins with SF-II MCs showed a marked enhancement at 20 wt% MC loading. Additional MC loading led to a decrease in resin strength. The results illustrate a fact that spherical MCs tend to improve the mechanical properties only at low MC loading. Earlier results suggested that adding any MCs decreases the resin strength [5, 6, 15]. These results are consistent with the SEM analysis (shown in Fig. 8) which showed clean surfaces of intact MCs on the fracture surfaces indicating that spherical SF-I MCs can compromise resin mechanical properties. The strength enhancement obtained in resins loaded with SF-II may be a result of their elongated shapes.

Figure 10 depicts the effect of different MC loadings on the toughness of resins in self-healing efficiency tests. Toughness was calculated as the area under the curve. Resins loaded with SF-I MCs showed a minor enhancement in toughness at all loading levels. In contrast, resins with SF-II MCs greatly improved

the toughness at 20 wt% loading compared to the control group. Toughness has been shown to increase by 8–10 folds in fiber-reinforced composites when cracks run parallel to fibers resulting in fiber/resin debonding [24]. The elongated MCs (SF-II) may be comparable to fibers to some extent and provide an energy-absorbing mechanism through MC/resin debonding, leading to toughness enhancement. Earlier research has stated that a rougher fracture surface compared to resins with SF-I MCs indicated a toughness effect brought by SF-II MCs, as shown in SEM images in Figs. 7 and 8 [25].

Figure 11 presents the effect of MC loading on resin modulus values obtained from the tensile tests. Resins loaded with SF-I MCs showed enhancement in Young's modulus. On the contrary, the modulus dropped from 25.14 MPa to 7.1 MPa with MCs from 5 wt% to 15 wt%, respectively. These results suggest, indirectly, that SF-I MCs may not be bonded well with the resin and are more likely to reduce the stiffness. Resins embedded with SF-II MCs reached a maximum modulus value of 147.6 MPa with 20 wt% loading. The modulus sharply decreased beyond 20 wt% MC loading. A possible explanation for this result is that overloaded MCs lead to aggregation at some locations. In the stress vs. strain plots shown in Figs. 11(b) and (c), it was noticed that the initial cracks propagated and eventually led to specimen failure as stress increased. In SF-I MC embedded resins, the fracture strains dropped as the MC loading increased, indicating that spherical MC loadings (SF-I) possibly introduced more defects, perhaps due to aggregation. This higher defect density contributed to the premature failure of samples. It is also possible that spherical MCs do not bond well to resin. The stress vs strain plots of SF-II MC containing resins showed similar characteristics but higher modulus as well as higher fracture strains. For SF-II MC embedded resins, there was an optimum loading of MC (20%) that yielded resins with the highest fracture strain in the range of 70%. It was assumed that randomly distributed elongated MCs can increase fracture strains as resins and MCs deform simultaneously and resin deformation around elongated MCs so that resin sustains stress till it reaches the fracture limits [25]. However, additional MCs beyond the optimum loading compromises the resin's properties.

3.7 Self-healing efficiency tests

Figure 12 presents the self-healing efficiencies of SPI resins in terms of strength recovery as well as toughness recovery for both resins containing SF-I and SF-II MCs and as a function of MC loadings. As expected, resins with higher MC loadings resulted in higher self-healing efficiency for both SF-I and SF-II MCs. Resins loaded with 15 wt% of SF-I MCs displayed the highest self-healing efficiency for strength recovery of 47.4% compared to 14.0% for virgin resin (without MCs) and 62.9% toughness recovery compared to 23.9% for virgin resin. In the case of SF-II MCs, the self-healing efficiency for strength recovery reached 44.8% and toughness recovery reached 40.6%. While self-healing efficiencies for resins with SF-I MCs are higher than resins containing SF-II MCs, this seems to be an artifact that results from the severely compromised mechanical properties of the resins containing SF-I MCs (as shown in Figs. 9 and 10). It was seen in Fig. 9 that the failure loads were significantly lower for resins containing SF-I MCs compared to those containing SF-II MCs. Also, Fig. 10 showed clearly that the toughness and modulus of resins with SF-I MCs was lower than those containing SF-II MCs.

The purpose of self-healing functionality is to recover the mechanical properties of the material by healing or bridging the microcracks that develop under stress to a level equivalent or even higher than their virgin values without compromising their properties as a result of MC addition. Considering what has been discussed above, it seems that spherical SF-I MCs act as defects in the resins and degrade their mechanical properties. As a result, it can be concluded that SF-I MCs may not be suitable as self-healing fillers in this case. Resins with SF-II MCs, presented in Fig. 12, showed a slight improvement in self-healing efficiency between MC loadings of 20 wt% (42.6%) and 30 wt% (44.8%) in terms of strength recovery, and 38.9% and 40.6%, for corresponding MC loadings, in terms of toughness recovery. Compared with other soy self-healing protein-based resins, an earlier study by Kim and Netravali had shown a self-healing efficiency of up to 48% but with declined mechanical properties [5]. Apart from soy-based protein resins, 72% fracture stress recovery was reported in the case of zein resins [15]. Starch-based self-healing resins have also been fabricated and a 66% strength recovery was observed [6].

4 Conclusions

Both spherical and elongated MCs were prepared via syringe-filter emulsification technique using W/O/W double-emulsion system. Use of the syringe-filter method resulted in a narrow distribution of SF-I MC diameters, ranging between 0.5 μm and 1.8 μm. However, SF-I MCs compromised the mechanical strength of the resins, probably because of the weak MC/resin adhesion and spherical shapes. Irregular-shaped SF-II MCs containing elongated, elliptical, dog-bone, and rod-like shapes were also produced using the syringe-filter method and turned out to be helpful in terms of mechanical reinforcement of the resin. The aspect ratios of elongated SF-II MCs reached as high as 20. MCs with high aspect ratios can be dually beneficial as they could act not only as healing elements but may also reinforce the resin. SF-II MC containing resins (20 wt%) reached the highest self-healing efficiencies at 44.8% and 40.6% in terms of strength recovery and toughness recovery, respectively. Soy-based resins are sustainable, yearly renewable, and fully biodegradable. Results of this study suggest that soy-based structural resins can be promising substitutes for petroleum-based resins.

Declarations

Acknowledgments

The use of the Cornell Center for Materials Research Shared Facilities, which are supported through the NSF MRSEC program (DMR-1719875), is acknowledged. Authors would also like to acknowledge the funding support of Tata Cornell Institute for materials used in this work.

Compliance with Ethical Standards:

Funding: This study was partially funded by a grant from Tata Cornell Institute as stated above.

Conflict of Interest: The authors declare that they have no conflict of interest.

References

1. Geyer R, Jambeck JR, Law KL (2017) Production, use, and fate of all plastics ever made. Sci Adv 3:e1700782. https://doi.org/10.1126/sciadv.1700782
2. Cavallo AJ, implications for World Oil Production Forecasts (2004) Hubbert's petroleum production model: an evaluation and. Natural Resources Research 2004 13:4 13:211–221. https://doi.org/10.1007/S11053-004-0129-2
3. García MC, Torre M, Marina ML, Laborda F (1997) Composition and Characterization of Soyabean and Related Products. Crit Rev Food Sci Nutr 37:361–391. https://doi.org/10.1080/10408399709527779
4. Kim JR, Netravali AN (2018) Self-Healing Green Polymers and Composites. Advanced Green Composites. John Wiley & Sons, Inc., Hoboken, NJ, USA, pp 135–185. https://doi.org/10.1002/9781119323327.ch7.
5. Kim JR, Netravali AN (2016) Self-Healing Properties of Protein Resin with Soy Protein Isolate-Loaded Poly($_{D,L}$-lactide-co-glycolide) Microcapsules. Adv Funct Mater 26:4786–4796. https://doi.org/10.1002/adfm
6. Kim JR, Netravali AN (2017) Self-healing starch-based 'green' thermoset resin. Polymer 117:150–159. https://doi.org/10.1016/j.polymer.2017.04.026
7. Mauldin TC, Kessler MR (2010) Self-healing polymers and composites. Int Mater Rev 55:317–346. https://doi.org/10.1179/095066010X12646898728408
8. Kukizaki M (2009) Shirasu porous glass (SPG) membrane emulsification in the absence of shear flow at the membrane surface: Influence of surfactant type and concentration, viscosities of dispersed and continuous phases, and transmembrane pressure. J Membr Sci 327:234–243. https://doi.org/10.1016/j.memsci.2008.11.026
9. Liu R, Huang SS, Wan YH et al (2006) Preparation of insulin-loaded PLA/PLGA microcapsules by a novel membrane emulsification method and its release in vitro. Colloids Surf B 51:30–38. https://doi.org/10.1016/j.colsurfb.2006.05.014
10. Fernandez-Avila C, Trujillo AJ (2016) Ultra-High Pressure Homogenization improves oxidative stability and interfacial properties of soy protein isolate-stabilized emulsions. Food Chem 209:104–113. https://doi.org/10.1016/J.FOODCHEM.2016.04.019
11. Taha A, Hu T, Zhang Z et al (2018) Effect of different oils and ultrasound emulsification conditions on the physicochemical properties of emulsions stabilized by soy protein isolate. Ultrason Sonochem 49:283–293. https://doi.org/10.1016/j.ultsonch.2018.08.020
12. Thompson KL, Mable CJ, Lane JA et al (2015) Preparation of pickering double emulsions using block copolymer worms. Langmuir 31:4137–4144. https://doi.org/10.1021/acs.langmuir.5b00741
13. Hatate Y, Ohta H, Uemura Y, et al (1997) Preparation of monodispersed polymeric microspheres for toner particles by the shirasu porous glass membrane emulsification technique. Journal of Applied

Polymer Science 64:1107–1113. https://doi.org/10.1002/(SICI)1097-4628(19970509)64:6<1107::AID-APP10>3.0.CO;2-T

14. Shi S, Netravali AN (2021) Bacterial cellulose integrated irregularly shaped microcapsules enhance self-healing efficiency and mechanical properties of green soy protein resins. Journal of Materials Science 56:12030–12047. https://doi.org/10.1007/S10853-021-06066-Y
15. Souzandeh H, Netravali AN (2019) Self-healing of 'green' thermoset zein resins with irregular shaped waxy maize starch-based/poly(D,L-lactic-co-glycolic acid) microcapsules. Composites Science and Technology 183:107831. https://doi.org/10.1016/j.compscitech.2019.107831
16. Murakami H, Kobayashi M, Takeuchi H, Kawashima Y (1999) Preparation of poly(dl-lactide-co-glycolide) nanoparticles by modified spontaneous emulsification solvent diffusion method. International Journal of Pharmaceutics 187:143–152. https://doi.org/10.1016/S0378-5173(99)00187-8
17. ASTM E647-00 Standard Test Method for Measurement of Fatigue Crack Growth Rates, (n.d.). https://www.astm.org/DATABASE.CART/HISTORICAL/E647-00.htm (accessed July 8, 2020).
18. Hora MS, Rana RK, Nunberg JH, et al (1990) Release of Human Serum Albumin from Poly(lactide-co-glycolide) Microspheres. Pharmaceutical Research: An Official Journal of the American Association of Pharmaceutical Scientists 7:1190–1194. https://doi.org/10.1023/A:1015948829632
19. White SR, Sottos NR, Geubelle PH, et al (2001) Autonomic healing of polymer composites. Nature 409:794–797. https://doi.org/10.1038/35057232
20. Paragkumar N T, Edith D, Six JL (2006) Surface characteristics of PLA and PLGA films. Applied Surface Science 253:2758–2764. https://doi.org/10.1016/j.apsusc.2006.05.047
21. Combs JD (2016) Surface FTIR Techniques to Analyze the Conformation of Proteins/ Peptides in H2O Environment. Journal of Physical Chemistry & Biophysics 6:. https://doi.org/10.4172/2161-0398.1000202
22. Paniagua-Michel J, Fathepure BZ (2019) Microbial consortia and biodegradation of petroleum hydrocarbons in marine environments. In: Microbial Action on Hydrocarbons. Springer Singapore, pp 1–20https://doi.org/10.1007/978-981-13-1840-5_1.
23. Prosanov IY, Matvienko AA (2010) Study of PVA thermal destruction by means of IR and Raman spectroscopy. Physics of the Solid State 52:2203–2206. https://doi.org/10.1134/S1063783410100318
24. Nikpur K, Chen YF, Kardos JL (1990) Fracture toughness of unidirectional short-fiber reinforced epoxy composites. Composites Science and Technology 38:175–191. https://doi.org/10.1016/0266-3538(90)90005-P
25. Guo P, Chen X, Gao X, et al (2007) Fabrication and mechanical properties of well-dispersed multiwalled carbon nanotubes/epoxy composites. Composites Science and Technology 67:3331–3337. https://doi.org/10.1016/J.COMPSCITECH.2007.03.026

Figures

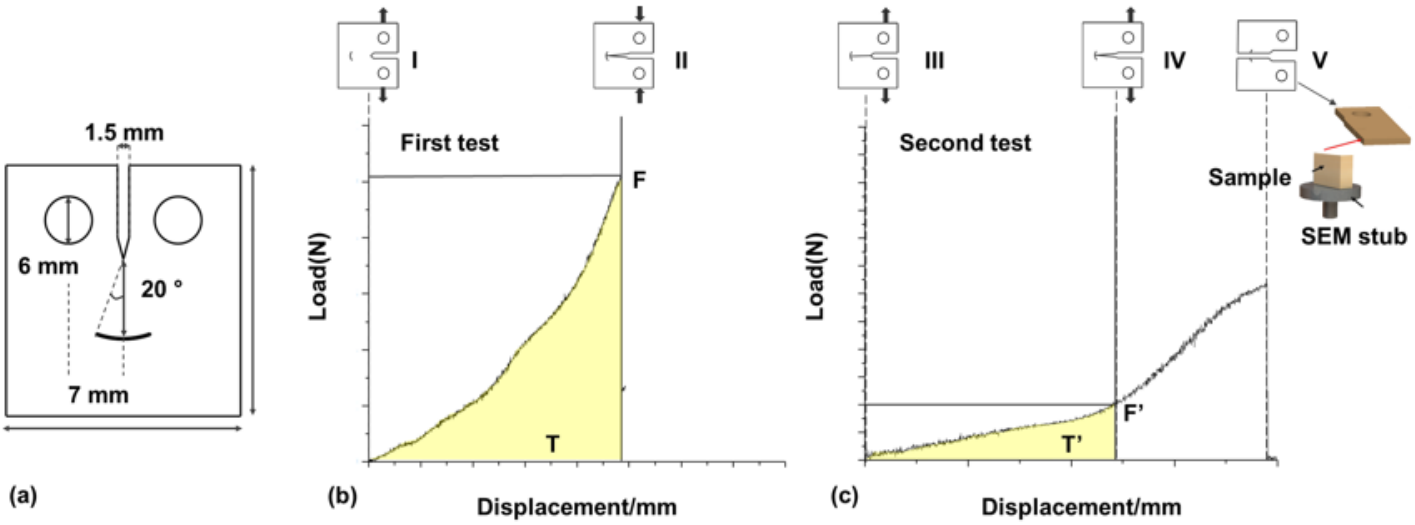

Figure 1

(a) Self-healing test specimen geometry; (b) and (c) load vs displacement plots obtained during typical self-healing tests [14].

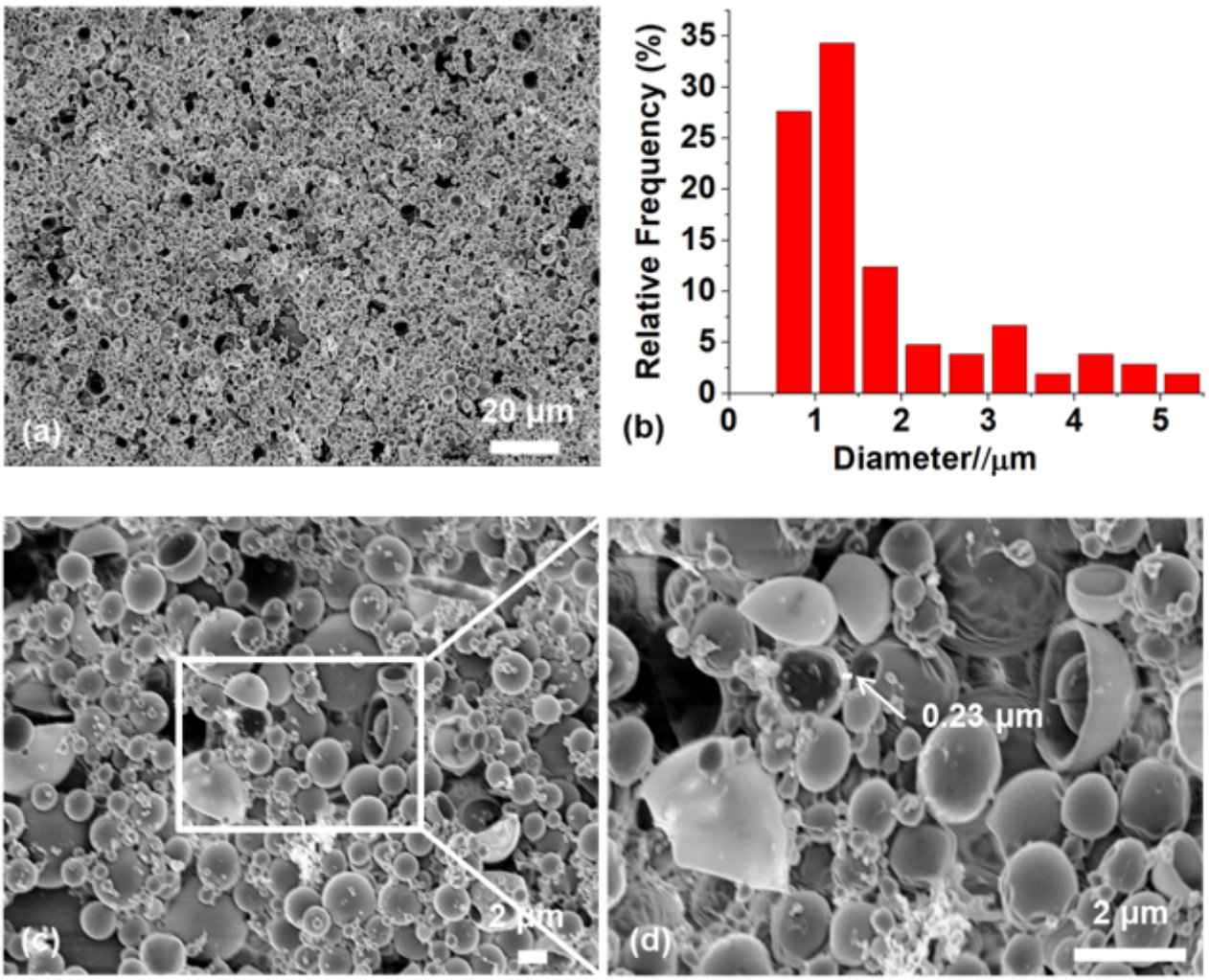

Figure 2

SEM images of SF-I SPI-PLGA MCs obtained via the syringe-filter method: (a), (c) and (d) are typical images of MCs. Figure (b) shows the size distribution histogram of spherical MCs.

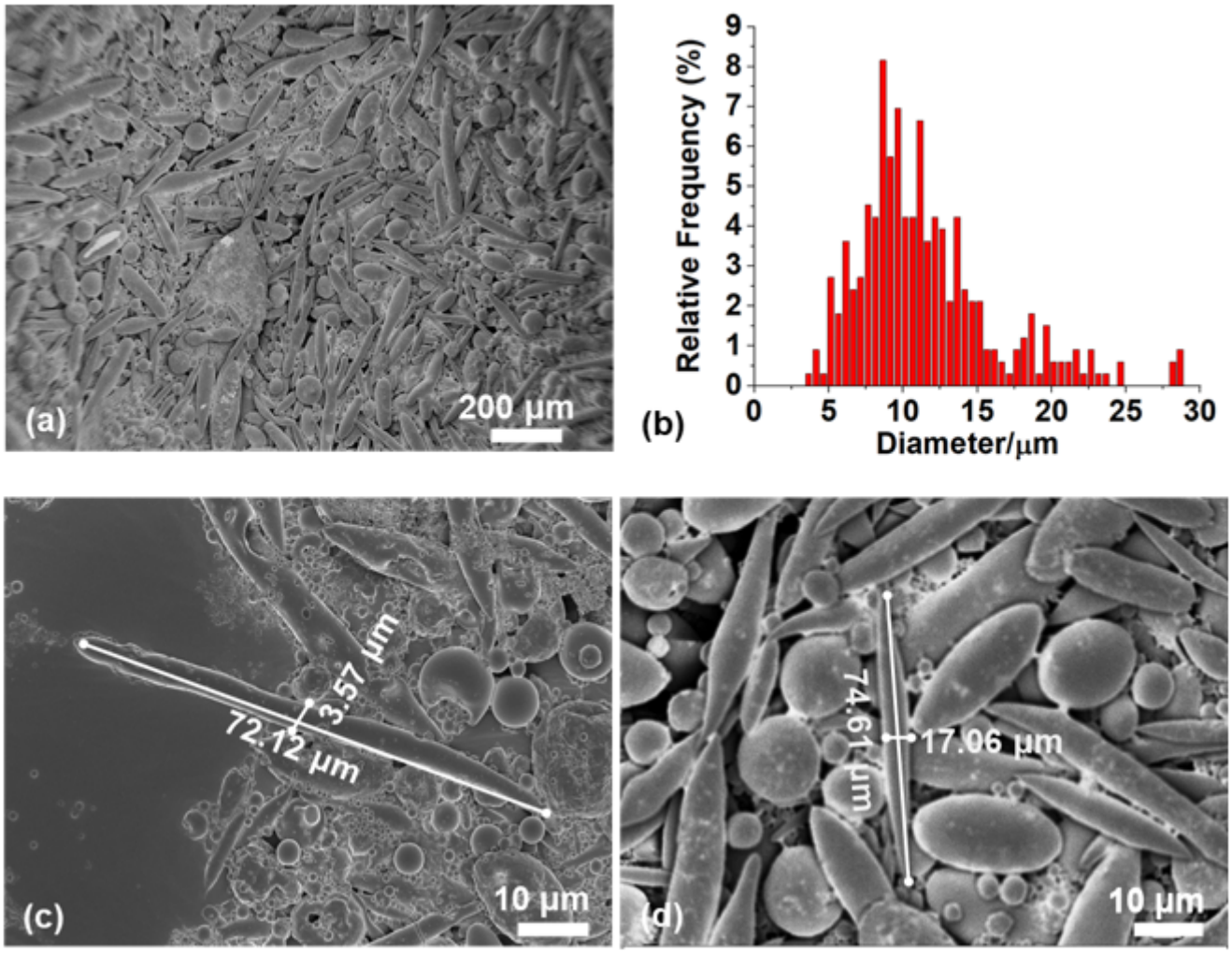

Figure 3

SEM images of SF-II SPI-PLGA MCs (a, c and d) were obtained via the syringe-filter method. Figure (b) shows the size distribution histogram of the MCs.

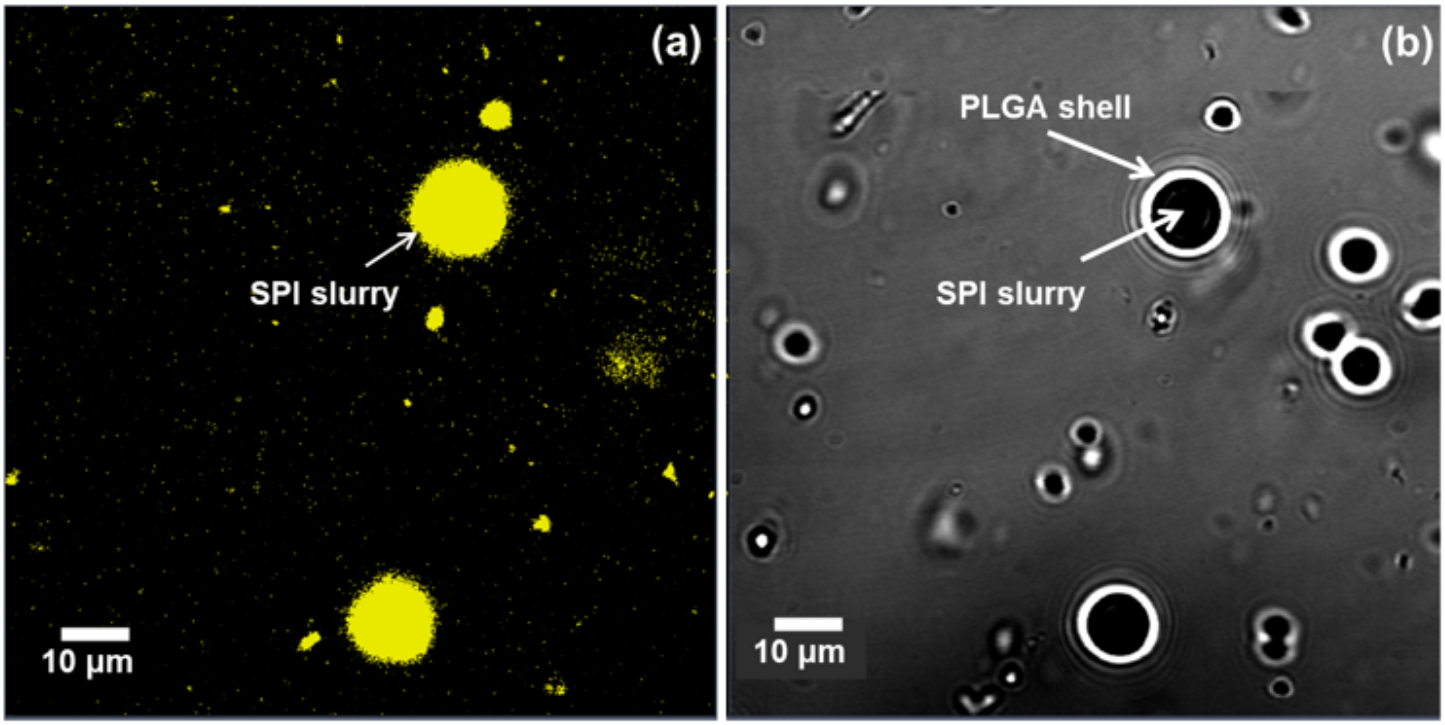

Figure 4

CLSM images showing the morphologies of SPI-PLGA SF-I MCs (a) fluorescent image and (b) image in transmission mode. The yellow color in the fluorescent image indicates the protein content.

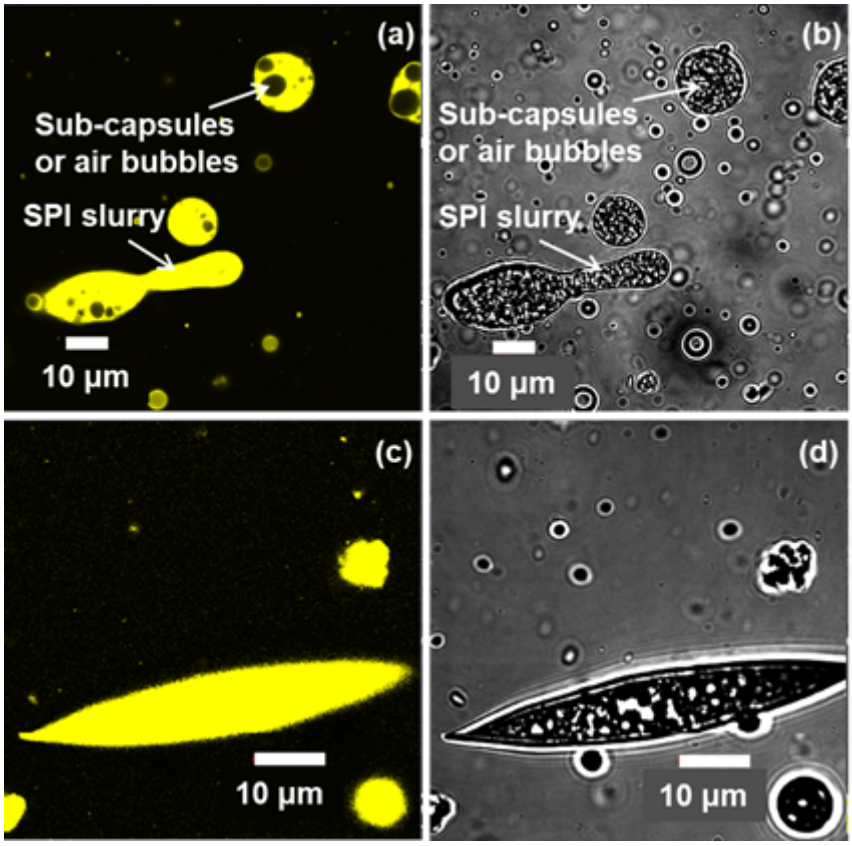

Figure 5

CLSM images showing the internal structures of elongated SPI-PLGA SF-II MCs: (a) and (c) are the fluorescent images and (b) and (d) are the images of MCs taken in transmission mode by CLSM. The yellow color indicates protein (mostly).

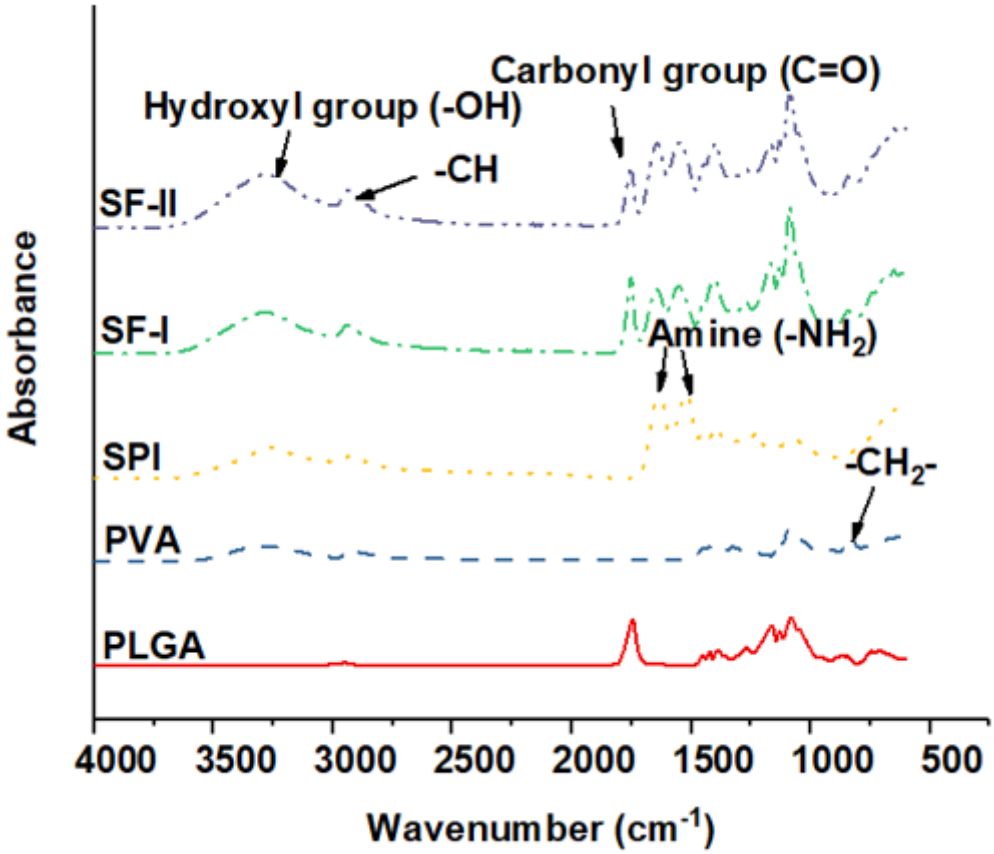

Figure 6

ATR-FTIR spectra of MCs, compared with PLGA, PVA, and SPI.

Figure 7

Typical SEM images of the fracture surfaces of SPI resins loaded with 15 wt% SF-I SPI-PLGA MCs.

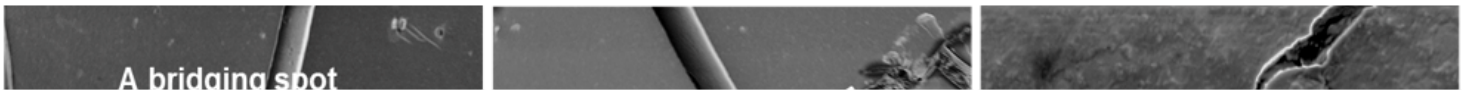

Figure 8

Typical SEM images of the fracture surfaces and crack sizes of SPI resins loaded with 30 wt% of SF-II SPI-PLGA MCs.

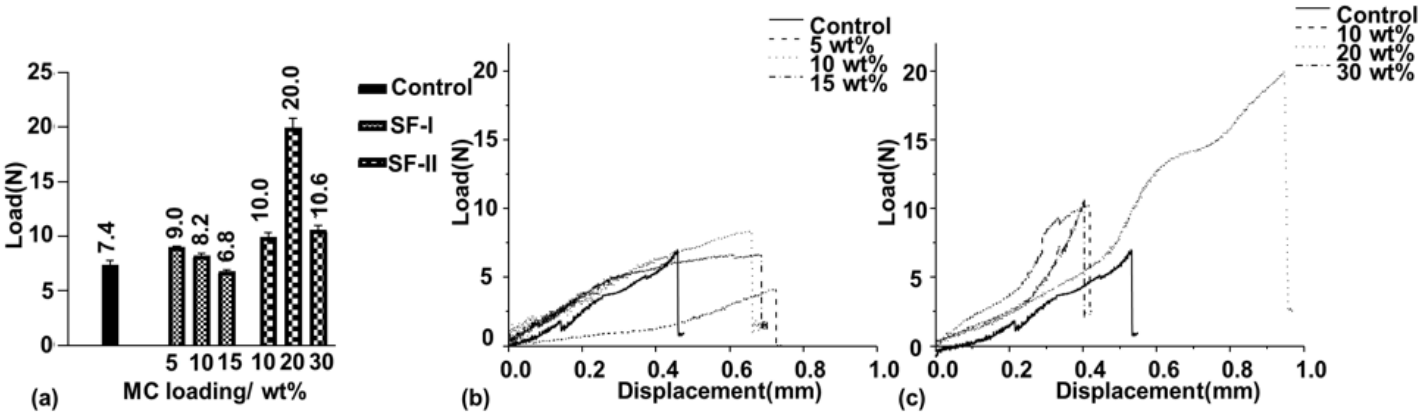

Figure 9

(a) Effect of MC loading on resin failure load in self-healing efficiency tests. Typical load vs displacement plots for (b) resins with SF-I MCs and (c) resins with SF-II MCs.

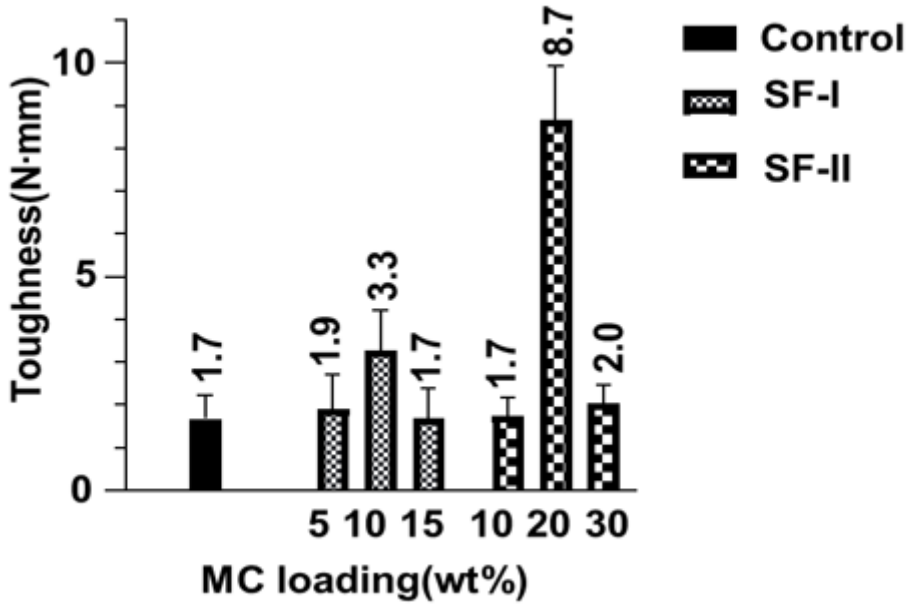

Figure 10

Effect of MC loading on the resin toughness in self-healing efficiency tests.

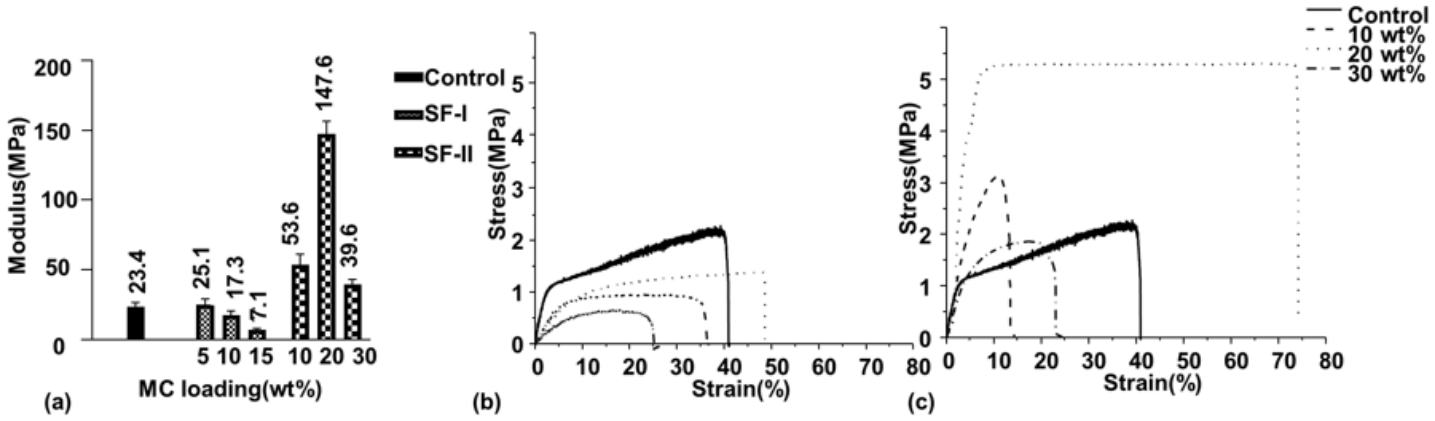

Figure 11

(a) Effect of MC loading on the resin modulus values obtained from the tensile tests. Typical strain vs stress plots in tensile tests with different MC loadings for (b) resins with SF-I MCs and (c) resins with SF-II MCs.

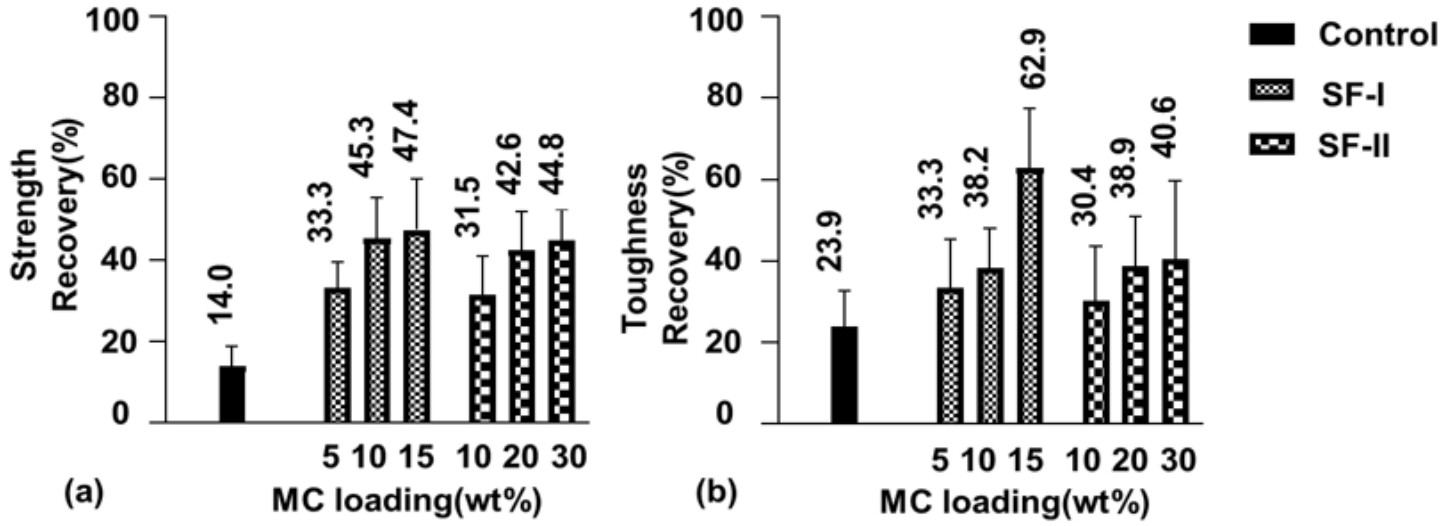

Figure 12

Self-healing efficiencies of SPI resins as a function of MC loadings: (a) self-healing efficiency based on strength recovery (resin failure load); (b) self-healing efficiency based on toughness recovery.